Experimentally Modeling the Behavior of a Hall-Effect Thruster at Atmospheric Pressure

Daniel O. Bonilla

Adviser: Dr. Robert Fersch

Christopher Newport University

Abstract

Aeronautic Hall-effect thrusters (AHET) – those that use atmospheric gases as ionic propellant – have little practical use other than demonstrating the behavior of various electrostatic systems. Because Hall-effect thrusters (HET) in general produce so little thrust, even the most powerful of them are almost useless in sub-orbital aviation; these Earthbound thrusters must overcome the influences of gravity and air resistance, forces that do not normally inhibit the behavior of spacecraft. However, if a specialized, mathematical model were to be identified, predicting the behavior of an AHET, it may provide a means for maximizing the thrust of the engine; with greater thrust, HETs may eventually become more practical for aeronautic application. The purpose of this experiment was to identify one such model, capable of estimating the thrust generated by the AHET as a function of the voltage supplied to it.

Currently, there are not many extant models that accurately predict the performance of AHETs. For that reason, the models used in this experiment were derived directly from relevant kinematic and electrostatic laws. The first, rudimentary model was compared to the experimentally measured thrust force, and it was found that there was, in fact, a direct, linear proportionality between the supplied voltage and the thrust generated. With that knowledge, further testing was performed to generate models with increasing accuracy of correlation to the experimental results. Over time, the goal of the project changed slightly to include a secondary hypothesis: despite the fundamental differences between each model, the similarities between them suggested that they, in fact, represented accurate physical predictions, while the data acquired during the experiment was flawed due to an unknown systematic error. Determining this source of error may only be possible by conducting further research beyond the immediate

scope of the project, but the results suggest that the final model, in particular, is potentially generalizable, insofar as predicting the behavior of other AHETs.

Introduction

The Hall-effect thruster (HET) is a type of ionic propulsion engine, a device that is almost exclusively used to drive the motion of small spacecraft. HETs achieve thrust by exposing a gaseous propellant (typically argon or xenon) to a powerful electric field, thus ionizing the propellant; the ions are themselves accelerated by the field, resulting in a net acceleration of the spacecraft. In terms of nomenclature, it is easy to confuse HETs with gridded ion thrusters (often referred to simply as ion thrusters). To clarify the distinction, HETs use an electric field to both ionize and accelerate the propellant, while gridded ion thrusters first ionize the propellant with an electron gun and then accelerate the ions through an electric field. Regardless, all ionic propulsion devices produce miniscule accelerations, but due to their unique hyper-efficiency, they can achieve enormous accelerations over long periods of time. For this reason, many small satellites and long distance probes are outfitted with such thrusters in order to maximize their Delta-V (total, possible change in velocity), potentially extending mission duration by years.

A specialized variant of Hall-effect thruster, dubbed the aeronautic Hall-effect thruster (AHET), was employed in this experiment. This was done not only to reduce the complexity of the experiment, but also because AHETs, by definition, function outside of a vacuum, using atmospheric oxygen and nitrogen as propellants, eliminating the need for onboard fuel or propellant storage.

The purpose of this project has been to model the behavior of HETs, specifically those designed to operate at atmospheric pressures. Being a more exploratory experiment, the intent was not to provide further support to an accepted theory or physical concept, but rather to identify – using various extant theories – an accurate mathematical model capable of predicting the behavior of any AHET. The expected result of the experiment was a formula indicative of the proportionality between the voltage supplied to the AHET and the thrust produced by it. All models used during the experiment were algebraically derived from various combinations of electrostatic and kinematic laws.

Theory

The underlying physics that allow the AHET to produce thrust are as follows. In electrostatics, the charge density on the surface of a conductor with converging radius of curvature, similar that in figure 1, will diverge as this radius approaches zero. Consequentially, the electric field produced at this infinitesimal point will diverge (Jackson, 1999, p. 94).

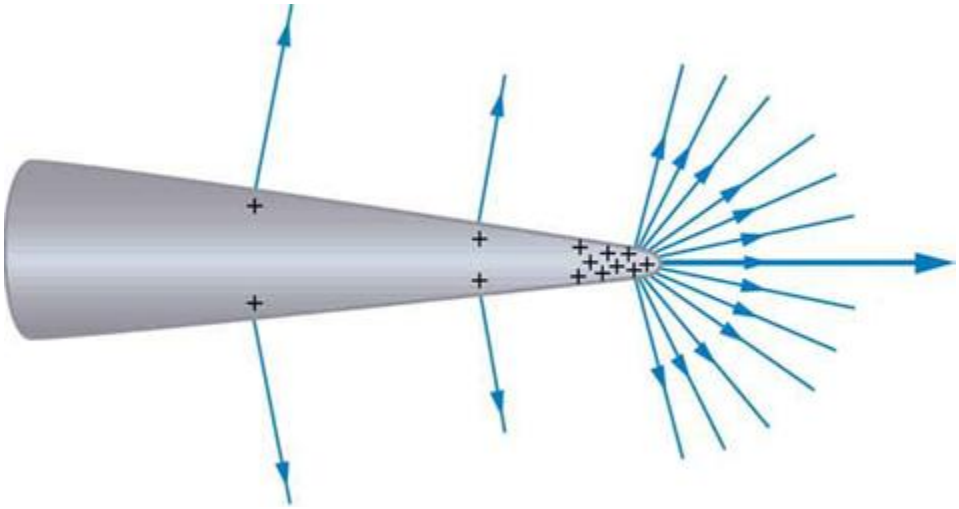

Figure 1: Conductor Charge Density & Radius of Curvature

If the tip of such a pointed conductor were to be directed at another with a more rounded face, one with high radius of curvature, and a high voltage were to be applied across them, the electric field lines would connect between these two electrodes. Assuming these electrodes were to be placed in a lab at atmospheric pressure, as the field increased, it would rip electrons away from the nitrogen and oxygen molecules in the air, thus converting them into positive ions, which would then accelerate in the direction of the electric field. As the ions accelerated, their fluidic viscosity would result in a momentum transfer to nearby, neutrally-charged particles resulting in a mass-flow towards the rounded electrode. The velocity of this ion wind could then be measured and used to calculate the force of thrust.

Before constructing a prototype ion engine, it was necessary to develop a rudimentary, working model capable of accurately predicting the force of thrust produced by this ionic reaction, and to allow for comparison with the measured data later in the project. The algebraic combination of Coulomb's Law for voltage:

$$\mathcal{V} = k_e \frac{q}{r} \quad \textbf{(1)}$$

the Law of Conservation of Energy:

$$\mathcal{U} = q\mathcal{V} = \frac{1}{2}mv^2 \quad \textbf{(2)}$$

and Tsiolkovsky's Generalized Rocket Equation:

$$F_T = \frac{dm}{dt}v \quad \textbf{(3)}$$

yielded the first working model for the expected thrust produced by the engine as a function of the effective voltage provided to it:

$$F_T(\mathcal{V}_e) = \frac{2nrE}{k_e}\mathcal{V}_e \quad \textbf{(}\boldsymbol{\alpha}\textbf{)}$$

Where n represents the number of individual ion engines included in the electrode array, r represents the radius of curvature of the tip of each copper nail in the array, E is the constant

that represents the electric breakdown field of air, k_e is Coulomb's constant, and $\mathcal{V}_e$ is one half of the route-mean-square (RMS) voltage; because the ion engine circuit operates using alternating current, the input voltage must be the RMS of the apparent input, and the alternating polarity only allows ion production one half of the time the circuit is active. For the sake of simplicity, this particular model was dubbed model $\boldsymbol{\alpha}$. Other models would later be used to more accurately reflect the experimental data, and the mathematics were largely similar to those used to develop $\boldsymbol{\alpha}$, at least in terms of the theories used. However, there were slight differences in terms of the relevant conceptual considerations. The first model, while not sufficiently accurate, provided a basis for experimental testing, specifically with regard to confirming the proportionality between voltage and thrust as both direct and linear.

Methods

Numerous AHET design variations were considered to ensure accurate data acquisition, most of which would have involved the engine assembly itself moving, much like a rocket. However, a stationary design was ultimately chosen for its relative simplicity of construction and the expected ease with which its force of thrust could be measured; in order to determine the thrust, it was far simpler to measure the motion of the propellant, as opposed to the motion of the AHET assembly. An additional benefit of employing the stationary assembly was a considerable reduction of the risk involved in the experiment; there was certainly a far greater chance of accidents occurring with the high voltage source moving quickly or unpredictably, as opposed to being a stationary, easily controllable assembly. Overall, there were still great risks in performing this experiment, but the stationary assembly made the dangerous high voltage components more containable, and thus, safer.

The early prototype AHET assemblies involved the use of wooden structures to support the engine electrodes, but for many reasons – design safety, precision, and aesthetic appeal being among them – the later designs were revised to instead use 3D printed structural supports. The primary inspiration for the design and execution can be credited both to Duarte (2015) and Reifsnyder (2015) for their comprehensive project guides.

The final prototype AHET (see Appendix D for pictures) used in this experiment consisted of a group of seven copper nails mounted on an adjustable 3D printed support structure facing an identical configuration of seven copper coupling tubes; one nail for each coupling, each pair forming an individual engine in the assembly, for a total of seven engines. The nails acted as the pointed electrodes in the electrostatic system, with minimum radius of curvature at the nail tips, while the coupling tubes acted as the rounded electrodes, with much larger total radii of curvature. Both halves of the electrode array were then wired to a high voltage Neon Sign Transformer (NST), which was then connected to a momentary-on, pressure switch, included as a failsafe to allow for a quick and easy method to cut off power to the NST. Power was supplied to this failsafe switch by a variable autotransformer, capable of modulating the output voltage on a continuous distribution from zero to the maximum 120V provided by a standard U.S. wall outlet (see Appendix A for final design blueprint and Appendix B for circuit schematic).

The autotransformer was used to modulate the input voltage through the NST, so that the voltage supplied to the AHET could be more easily regulated. As the variable transformer output was raised, the engine would appear to ionize increasing quantities of the air between the electrodes, a process that was qualitatively observable even in the early prototype designs, indicated by a faint plasma-glow. With the variable power provided by the autotransformer, the

NST produced an estimated maximum voltage of 12kV at a current of 35mA, but to reiterate, this was an alternating current circuit, so the actual *effective* voltage across the engine electrodes was one half of the route-mean-square of the NST output, approximately 4kV; the polarity would alternate at a rate of 60Hz, and the production of ion wind was only possible so long as the nails bore the positive pole, occurring one half of the time the circuit was active. The available project resources, regrettably did not include voltmeters that were designed to handle voltages higher than even 1kV, so the only available means of determining the actual voltage supplied by the NST was to extrapolate the value based on the input voltage provided by the autotransformer.

To prepare the AHET elements, a long copper tube was cut into seven couplings of equal length, which were spun on a rotary lathe to ensure uniform precision. The couplings were then each polished clean, coated with solder flux paste, and arranged in a hexagonal honeycomb pattern. The tubes were then soldered together with a blowtorch in the same honeycomb pattern and subsequently soldered to a long segment of 18 gauge, solid copper wire. Once this was done, the structural components (as shown in Appendix A) were printed using a MakerBot 2X 3D printing platform, and the honeycomb shaped coupling array was mounted on these supports, along with seven nails in the slots facing the coupling array.

Following the construction of the AHET, a shielded housing was installed to contain the device. The intent was to prevent the device's operator being exposed to any of the high voltage components, particularly the engine input leads, which had to be largely uninsulated to properly provide power. Ultimately, these high voltage components were all sealed in an acrylic containment unit to eliminate the possibility of any accidents occurring. It was also found that, whenever operated, the device produced a massive quantity of ozone as a result of the ionization reaction; ozone can be very dangerous to one's health, particularly in the long term. Fortunately,

the testing assembly was sufficiently compact, so the whole apparatus could be installed inside a fume hood, allowing ozone to be safely evacuated from the chamber, protecting the operator of the AHET (see Appendix C for full list of fabrication materials and testing resources).

Ultimately, the ion wind generated by the AHET would pass through the copper coupling tubes, subsequently through a 3D printed tube or nozzle to confine the air flow, and finally through an anemometer sensor that would actively read out the immediate velocity of the wind, the value of which could be used to calculate the force of thrust that correlated with the relevant input voltage. A slightly altered variant of Tsiolkovsky's Generalized Rocket Equation was used to calculate the thrust as a function of the measured ion wind velocity.

$$F_T(v) = \rho \pi R^2 v^2 \quad \textbf{(4)}$$

Where ρ is the density of air at the relevant lab temperature and pressure, and R is the radius of the anemometer vane through which the ion wind passes as it exits the engine. After the initial testing, it was apparent that the anemometer vane would only respond to a particular, minimum ion wind velocity, thus the voltage was decremented from 100% to maximize the distribution of velocities that the anemometer could register. The voltage input to the engine was modulated using the autotransformer, decrementing from 100% to 70% of the maximum (again, approximately 4kV of effective input), in intervals of 2% for each distinct trial.

Data

Using equation 4, the ion wind velocities measured by the anemometer allowed for the calculation of thrust at each distinct voltage setting (sixteen total settings). This calculation yielded the following linear distribution, scatter plot:

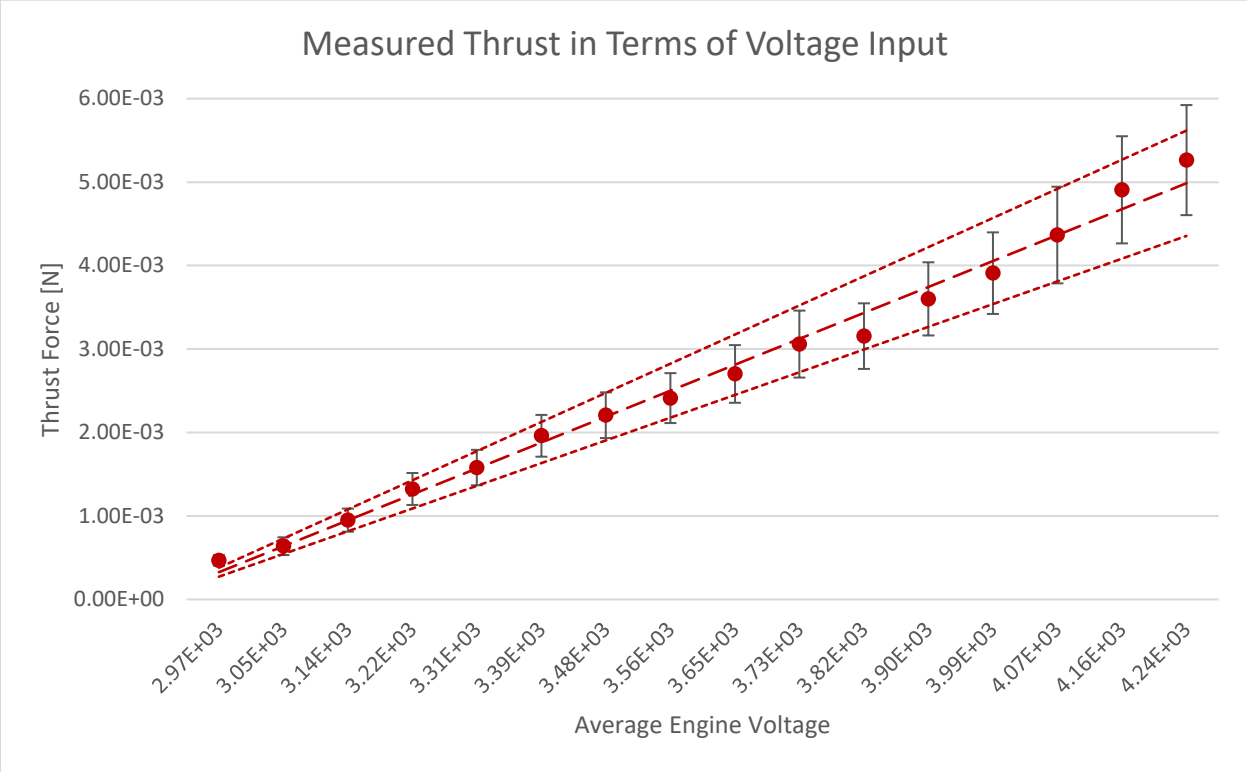

Figure 2

Figure 2 shows that there was, in fact, a direct, linear proportionality between the voltage supplied to the AHET and the thrust it produced. The central, dashed line is the linear fit of all sixteen data points, and the dotted lines above and below the central line represent the range of standard deviation in the thrust value. The plot seems to suggest that as the thrust increased, so too did the uncertainty in its measurement. In order to diagnose the cause of this behavior, further statistical analysis had to be performed.

As previously stated, the thrust as a function of ion wind velocity was calculated using equation 4, in which the velocity, radius, and air density each contributed some amount of uncertainty. The uncertainties in both velocity and density were determined using the variance in the measurements taken of their respective quantities; the average air density in the lab was found to be $(1.186 \pm 0.012)\ \mathrm{kg \cdot m^{-3}}$, while the average velocity – at 100% voltage input – was measured at $(1.214 \pm 0.008)\ \mathrm{m \cdot s^{-1}}$. The uncertainty in the radius was simply determined using the inherent uncertainty of the measurement device, in this case, a ruler, and the value was found to be $(3.10\times10^{-2} \pm 3.21\times10^{-3})$ m. At maximum voltage input to the AHET, the result is a peak thrust of $(5.26\times10^{-3} \pm 6.59\times10^{-4})$ N.

On average, the approximate uncertainty contributions of the air density and ion wind velocity measurements were both 8%, while the approximate contribution of the anemometer vane radius measurement was 84%, so a vast majority of the uncertainty in the thrust could be attributed to the measurement of this radius. It is still unclear why the uncertainty increases so dramatically with the thrust, but what is clear is that measuring the anemometer vane's radius more precisely could have reduced much of this uncertainty.

To assess the accuracy of the $\boldsymbol{\alpha}$ model, the thrust data was plotted alongside the theoretical predictions, with the following result:

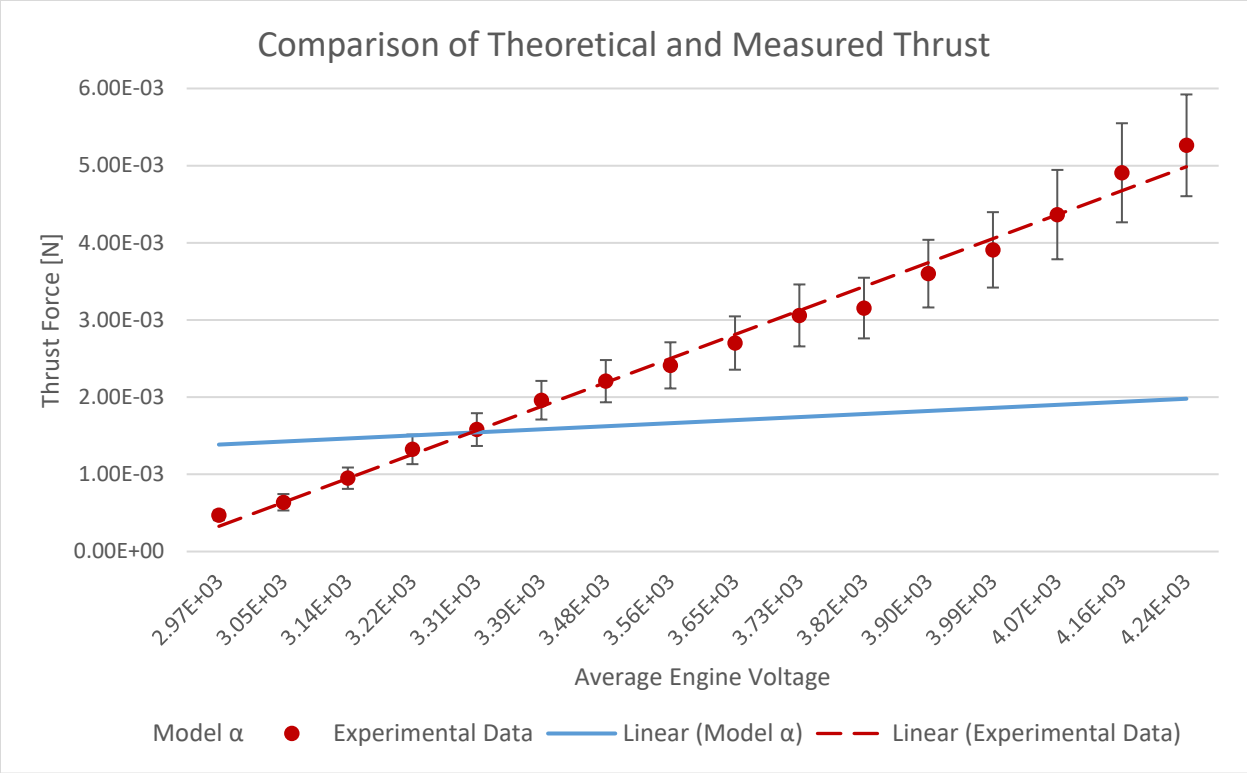

Figure 3

In figure 3, model $\boldsymbol{\alpha}$ is represented by the solid blue line, and the data is again represented by the dashed red line. In order to *mathematically* evaluate the model's accuracy, the average percentage difference was calculated between the model and the data. Percentage difference was used in place of percentage error because the latter requires that there is some firmly defined, accepted quantity with which to compare the measured quantity; because of the nature of the experiment, neither the data nor the models can be considered infallible, so the percentage difference was used for all data analysis comparisons. The average percentage difference between the data and model $\boldsymbol{\alpha}$ was found to be 54%, meaning that there was still substantial progress to be made towards maximizing the model's accuracy. Thus, a new model, $\boldsymbol{\beta}$, was developed using a similar foundation to that of model $\boldsymbol{\alpha}$. Both the rocket equation and

conservation of energy were again included, but where Coulomb's Law had been used in the development of $\boldsymbol{\alpha}$, the mass-flow rate formula was instead used to develop the new model:

$$\frac{dm}{dt} = \rho_\varepsilon \pi R^2 v_i \quad \textbf{(5)}$$

Model $\boldsymbol{\beta}$, like $\boldsymbol{\alpha}$ was also meant to predict the force of thrust produced as a function of the effective voltage input. When equations 1, 2, and 5 are algebraically combined, they result in the following:

$$F_T(\mathcal{V}_e) = 2nq_i\rho_\varepsilon \pi R^2 \mathcal{V}_e \quad (\boldsymbol{\beta})$$

Where n, again represents the number of individual ion engines included in the electrode array, q_i represents the charge of a single ion produced by the engine (assuming only one electron was removed in the creation of each ion, this charge must be the fundamental electron charge), ρ_ε is the estimated *number* density of ions produced in the reaction relative to the density of the neutral molecules nearby, and R is the radius of the anemometer vane through which the ion wind passes.

Initially, the linear plot of $\boldsymbol{\beta}$ had little similarity to that of the line for the experimental data. However, the $\boldsymbol{\beta}$ model was developed with several improvements over $\boldsymbol{\alpha}$, namely the inclusion of the constant, ρ_ε. The presence of this constant allowed for fine-tuning of the model, particularly the added ability to adjust the curve to correlate more accurately with the expected thrust values. This estimated ionic number density was calculated using the following relation:

$$\rho_\varepsilon = \varepsilon \frac{\rho}{m_i} \quad \textbf{(6)}$$

Where ε is the estimated efficiency of ion production, ρ is the density of air at the relevant lab temperature and pressure, and m_i is the approximate mass of a single ion, calculated using the average atomic mass of air (atmospheric nitrogen and oxygen). Ultimately, by

adjusting the efficiency term, it was possible to fine-tune the model to correlate more accurately with the data. With an estimated efficiency of 4.5ppm (an average of 4.5 ions produced out of every one million neutral air molecules), when the $\boldsymbol{\beta}$ model and data were plotted together, the result was the following:

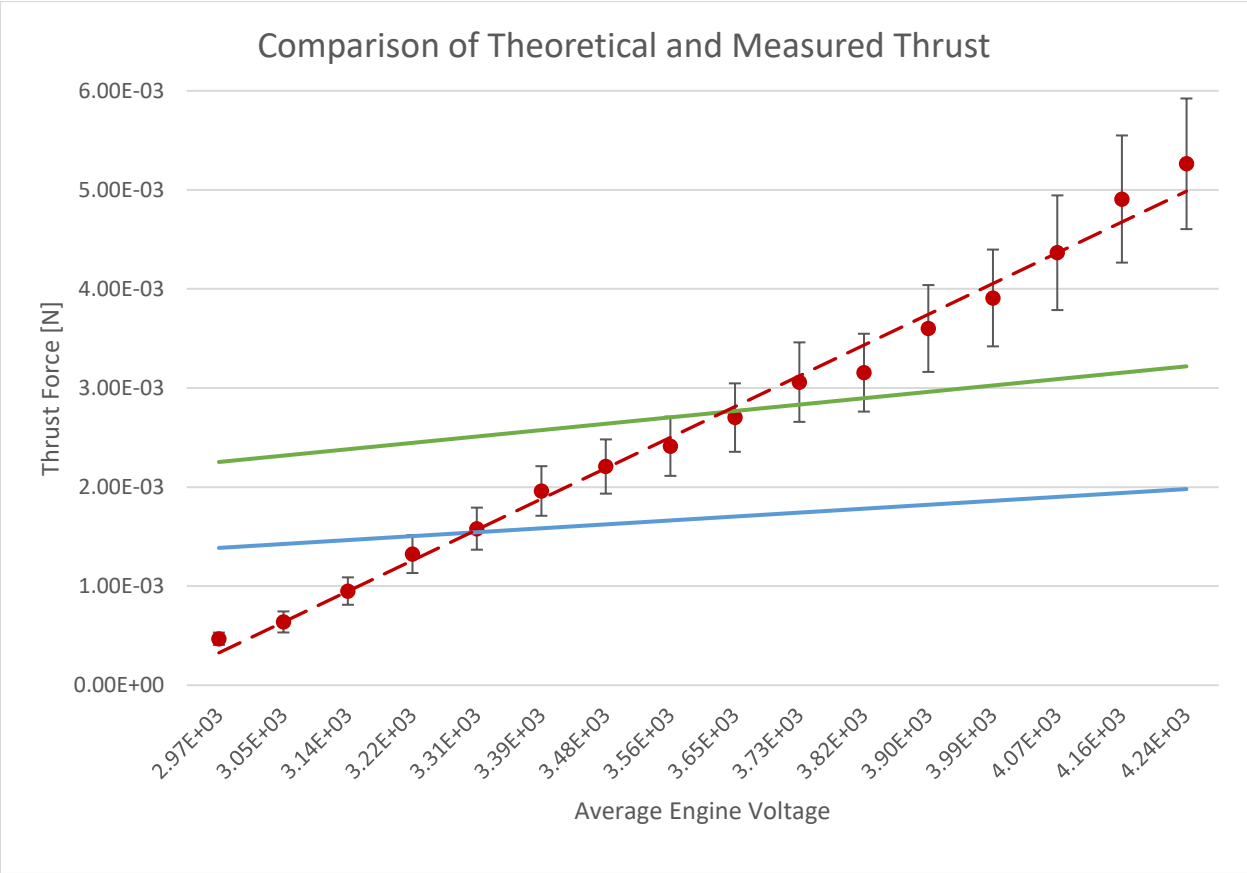

Figure 4

As shown in figure 4, the plots of both the experimental data (red) and $\boldsymbol{\beta}$ (green) show a slight improvement in similarity over model $\boldsymbol{\alpha}$ (light blue). The model comparison yielded an improved approximate percentage difference of 43% with the data. There was still, however, a notable offset between the two curves; the fact was that both models predicted the slope of the data line to be significantly shallower than what was measured. However, it is important to note the inherent oversight with the $\boldsymbol{\beta}$ model: while it certainly appeared to yield a more accurate

prediction to the experimental results, a great deal of "brute-forcing" was required to accomplish this; the efficiency term was useful for adjusting the model, but the actual value was heavily estimated, so there may not have been much significance to the apparent accuracy of the $\boldsymbol{\beta}$ model. If, however, the problem lay in some form of systematic error in the experimental results, then none of the models were necessarily inaccurate. The goal from then on was to develop more evidence supporting the claim that the flaw lay with the data, not the models.

Because of the deficiencies in $\boldsymbol{\beta}$, further attempts were then made toward developing yet another mathematical model. Similarly to $\boldsymbol{\alpha}$, the third model, $\boldsymbol{\gamma}$, was developed using the algebraic combination of the law of conservation of energy and Coulomb's Law, but in place of the generalized rocket equation, the power formula for rocket engines was used instead:

$$\frac{dm}{dt} = \frac{2\overline{P}_e}{v^2} \tag{7}$$

When combined with equations 1 and 2, the result was the force of thrust as a function of both voltage and current:

$$F_T(I_e, \mathcal{V}_e) = 2nI_e\sqrt{\frac{m_i\mathcal{V}_e}{2q_i}} \tag{$\boldsymbol{\gamma}$}$$

Where n, again represents the number of individual ion engines included in the electrode array, I_e is the effective current (one half the RMS current) provided to the AHET, m_i is again the approximate mass of a single ion, $\mathcal{V}_e$ is again the effective voltage across the AHET electrodes, and q_i again represents the charge of a single ion produced by the engine. The inclusion of I_e did establish the force as a function of power, not strictly voltage, but the variation in the value of this current was small enough that the plot of $\boldsymbol{\gamma}$ could be approximated as a linear function:

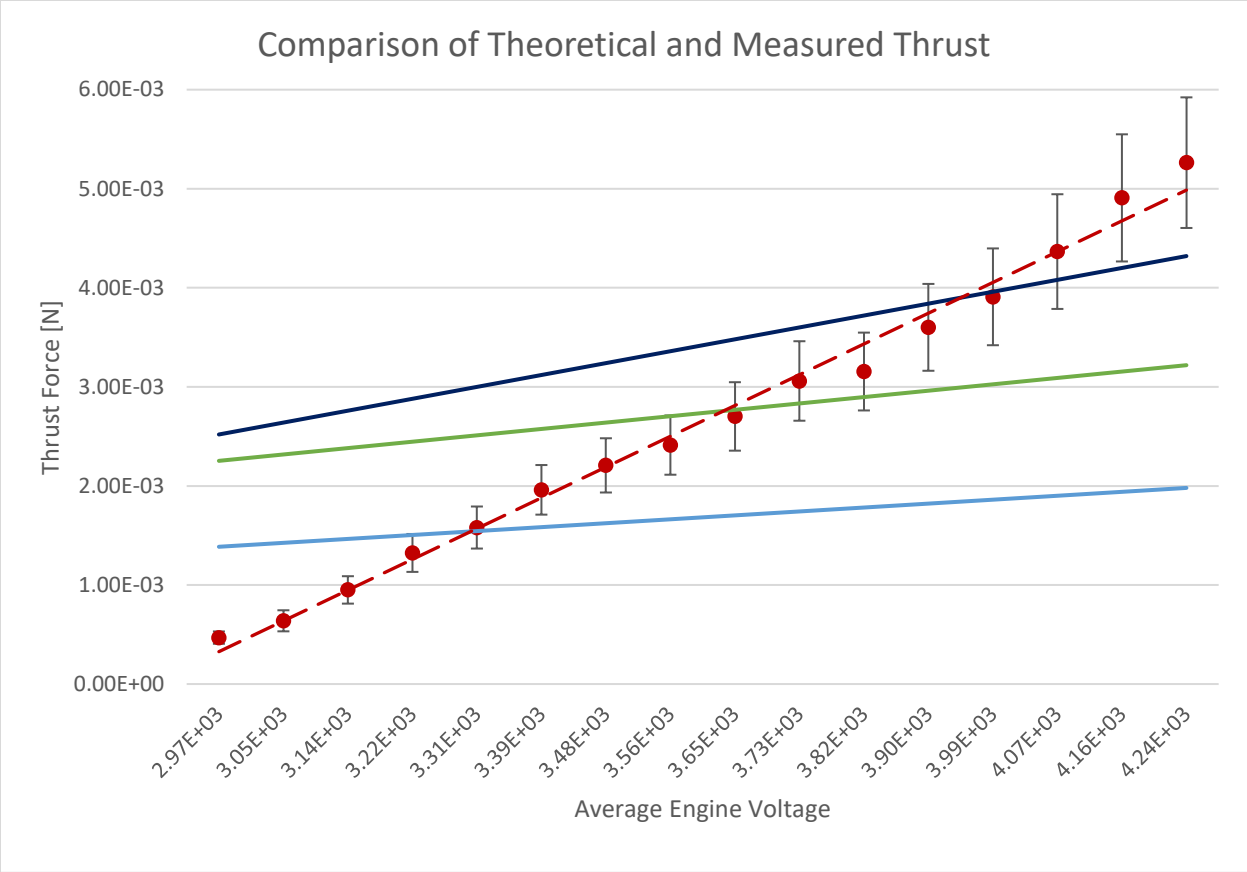

Figure 5

Figure 5 displays the comparison between the thrust data (red) and model $\boldsymbol{\gamma}$ (dark blue), but $\boldsymbol{\alpha}$ (light blue) and $\boldsymbol{\beta}$ (green) were also included to illustrate the distinction between all models. The approximate percentage difference between the data and model $\boldsymbol{\gamma}$ was 45%, slightly greater than that for $\boldsymbol{\beta}$. To address this decrease in accuracy presented by the $\boldsymbol{\gamma}$ model, a "hybrid" approach of sorts was taken to produce the fourth model. Fortunately, after a great deal of time spent searching for further information on ion engines in general, an immensely useful resource (Goebel, 2008) was located that provided, amongst other things, the derivation of another model. This fourth model, $\boldsymbol{\delta}$, was ultimately identical to $\boldsymbol{\gamma}$, with one exception, the inclusion of a scaling factor, meant to correct for various sources of thrust loss, much like the inclusion of the efficiency factor in $\boldsymbol{\beta}$. Hence, $\boldsymbol{\delta}$ is effectively a hybrid of the earlier models,

adopting the form of $\boldsymbol{\gamma}$ and the scaling factor concept from $\boldsymbol{\beta}$. The value of the *total* thrust correction, χ, is determined using two, distinct correction terms:

$$f = \cos\theta \tag{8}$$

Where θ is the half-angle divergence of the ion wind exiting the thruster, and f can be referred to as the divergence correction term;

$$\mu_s = \frac{1 + \frac{\sqrt{2}}{2}\frac{I^{++}}{I^{+}}}{1 + \frac{I^{++}}{I^{+}}} \tag{9}$$

Where I^{+} is the current due to singly charged ions (molecules with only one electron missing), and I^{++} is the current due to doubly charged ions. The term, μ_s can be referred to as the ion species correction term (Goebel, 2008, p. 22-24). So, the total correction factor will be:

$$\chi = \mu_s f \tag{10}$$

Due to the project's time constraints, the correction term values could not be measured directly, however χ could still be estimated for inclusion in the model. Ultimately:

$$F_T(I_e, \mathcal{V}_e) = 2n\chi I_e\sqrt{\frac{m_i \mathcal{V}_e}{2q_i}} \tag{$\boldsymbol{\delta}$}$$

Again with almost identical form to $\boldsymbol{\gamma}$, aside from the inclusion of the scaling factor. Approximating the model as a linear function of voltage, and using $\chi = 0.78$, the result is the following plot:

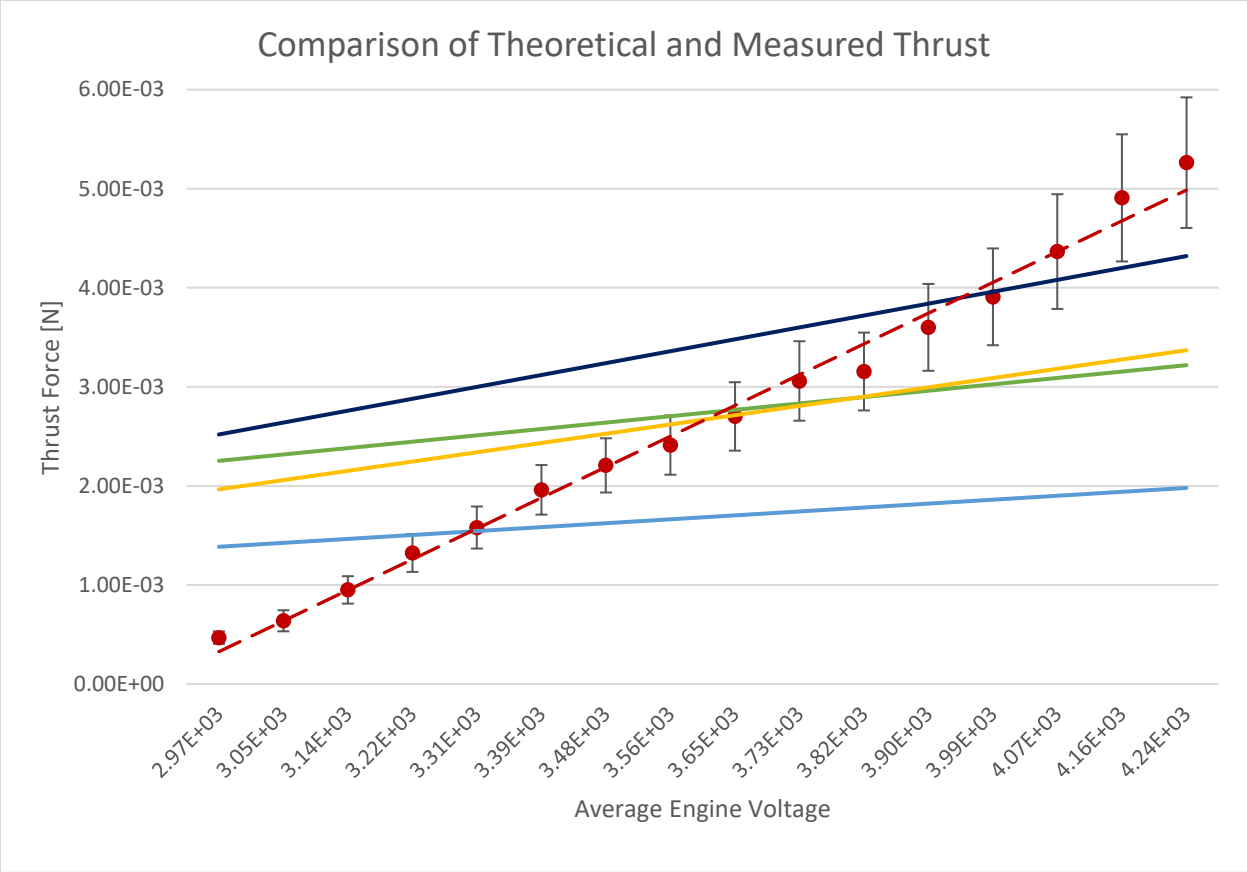

Figure 6

Figure 6 displays the experimental data (red) alongside all four models, $\boldsymbol{\alpha}$ (light blue), $\boldsymbol{\beta}$ (green), $\boldsymbol{\gamma}$ (dark blue), and $\boldsymbol{\delta}$ (yellow). The percentage difference for $\boldsymbol{\delta}$ was found to be 38% with respect to the data, the smallest difference calculated out of all other models. It is essential to recognize that the value of χ was not chosen randomly; much like what had been done for model $\boldsymbol{\beta}$, the scaling factor was chosen on the pretext of minimizing the percentage difference. Forcing a value for χ was not ideal, but again, there was limited project time to devote to directly measuring its value, not to mention limited testing resources, such as the instruments that would have been needed to measure the angle of ion wind divergence exiting the engine.

Conclusions

To reiterate, the initial acquired data suggested that the $\boldsymbol{\alpha}$ model was not sufficiently accurate, so a new model was developed. The $\boldsymbol{\beta}$ model, while built upon the same theoretical foundation as the first, included one key assumption to enhance the degree of correlation with the data, a scaling factor dependent on the efficiency of ion production in the engine. Subsequently, in an effort to support the validity of the models in general, model $\boldsymbol{\gamma}$ was produced, followed closely by model $\boldsymbol{\delta}$, which was identical to its predecessor, but like $\boldsymbol{\beta}$, included a scaling factor. Some amount of "brute-forcing" of the scaling factors was necessary to achieve proper correlation, but there is evidence to support the liberal adjustment of their values. All four models, while fundamentally different, collectively serve an important purpose; the models are highly similar to one another in terms of slope and general behavior, a fact that supports the hypothesis that the data itself is flawed due to some form of systematic error in its acquisition. As of the completion of the project, the following conclusions can be made:

1. There is a direct proportionality between the engine input voltage and the thrust it produces;
2. There is a linear relationship between the engine input voltage and the thrust;
3. The mathematical models correlate well with one another, but due to an unknown source of systematic error in data acquisition, the slope of the data's linear fit is far too high

Beyond these conclusions, little else can currently be said about how well the model correlates with the data. For instance, it was reasonable to conclude that the data was being affected by some systematic error, but unfortunately, there was not enough time before the conclusion of the project to investigate the actual source of that error. As it stands, the model is incomplete, and thus, would benefit greatly from further scrutiny and experimentation, however,

at the very least it provides an excellent platform for such research to build upon. Any further refinement of the model would require additional research that could potentially constitute an entirely new experiment, in and of itself. Therefore, the project, within its originally intended scope, can be considered a success, and the latest model predicting thrust as a function of the voltage provided to the aeronautic Hall-effect thruster can be considered accurate and potentially generalizable.

Appendix A: Ion Engine Assembly Blueprint

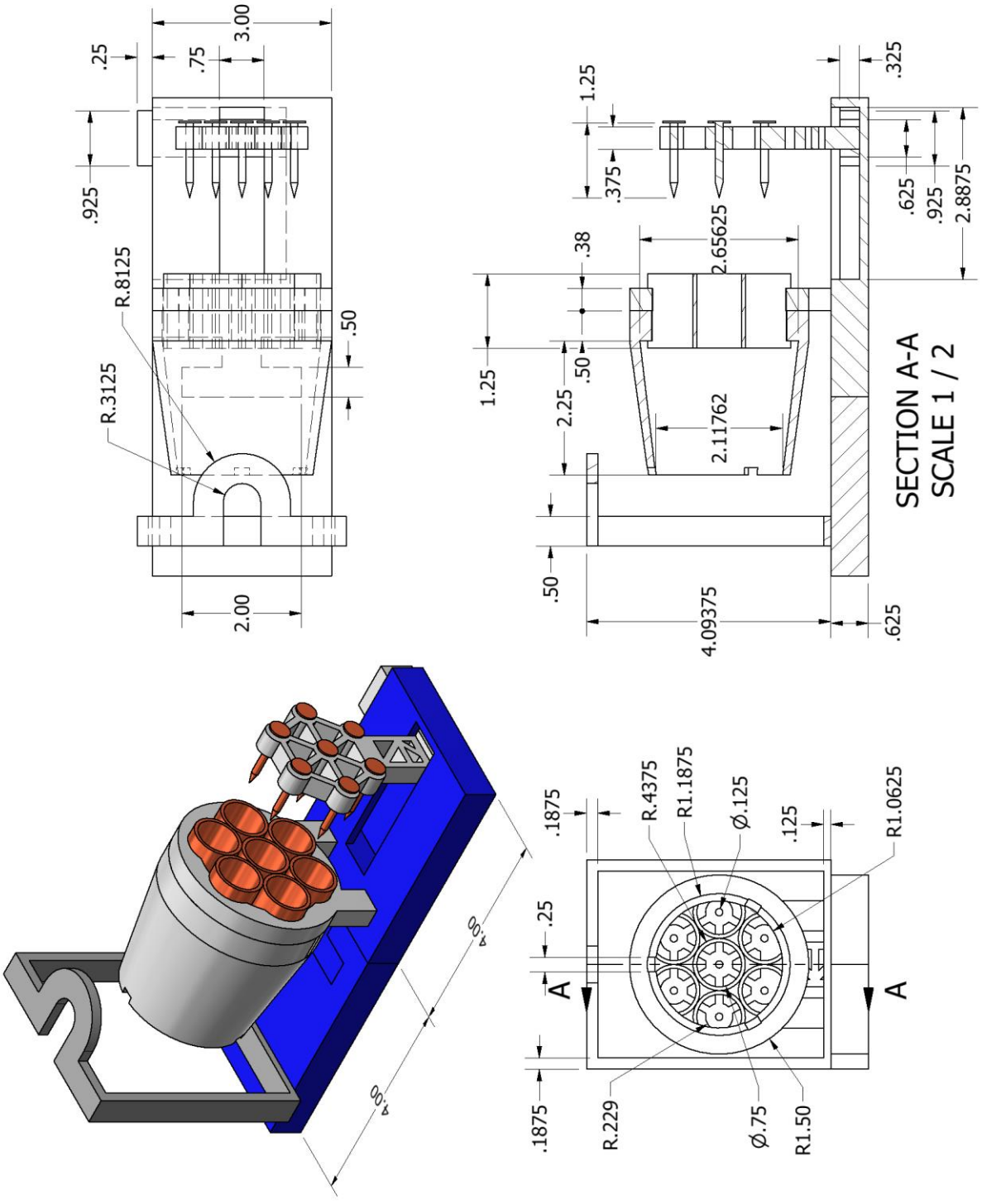

Appendix B: Ion Engine Assembly Circuit Schematic

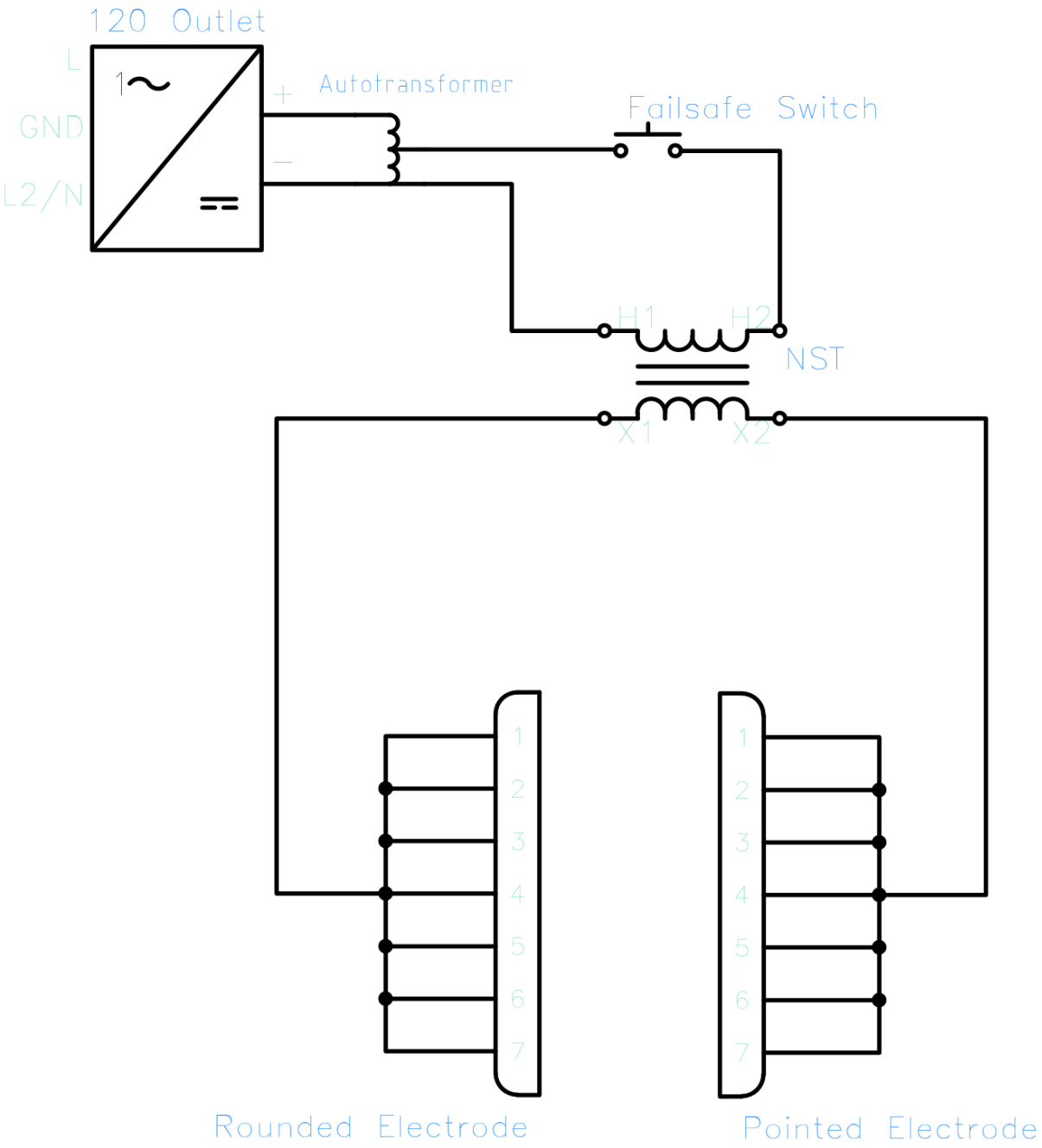

Appendix C: Materials and Resources

- Engine Testing Assembly Components
  - Neon Sign Transformer w/o Ground Fault Interference (GFI) Protection (12kV source at 35mA)
  - Variable Autotransformer (0-120V)
  - Momentary-on, Pressure Switch
  - Rotary Vane Anemometer Sensor
  - 1.0” Plywood Sheet (for testing assembly mounting platform)
  - Fume-hood (for evacuating noxious vapors and providing secondary protection from high-voltage components)
- Ion Engine Assembly Components
  - 7x 0.75” Diameter, Copper Couplings (0.5” diameter couplings were also used for the smaller engine)
  - 7x 0.125” Diameter, Solid Copper (or copper plated) Nails
  - 18 Gauge, Bare, Solid Copper Wire
  - 4x High Voltage Alligator Clips
  - Plumbing Solder
  - Solder Flux Paste
- Miscellaneous Manufacturing Resources
  - Blowtorch
  - Sandpaper (for smoothing out imperfections in 3D printed parts)
  - Acetone (for cleaning copper components)
  - MakerBot-2X 3D Printing Platform
  - Rotary Lathe

Appendix D: Final Prototype, Ionic Propulsion Engine Testing Platform

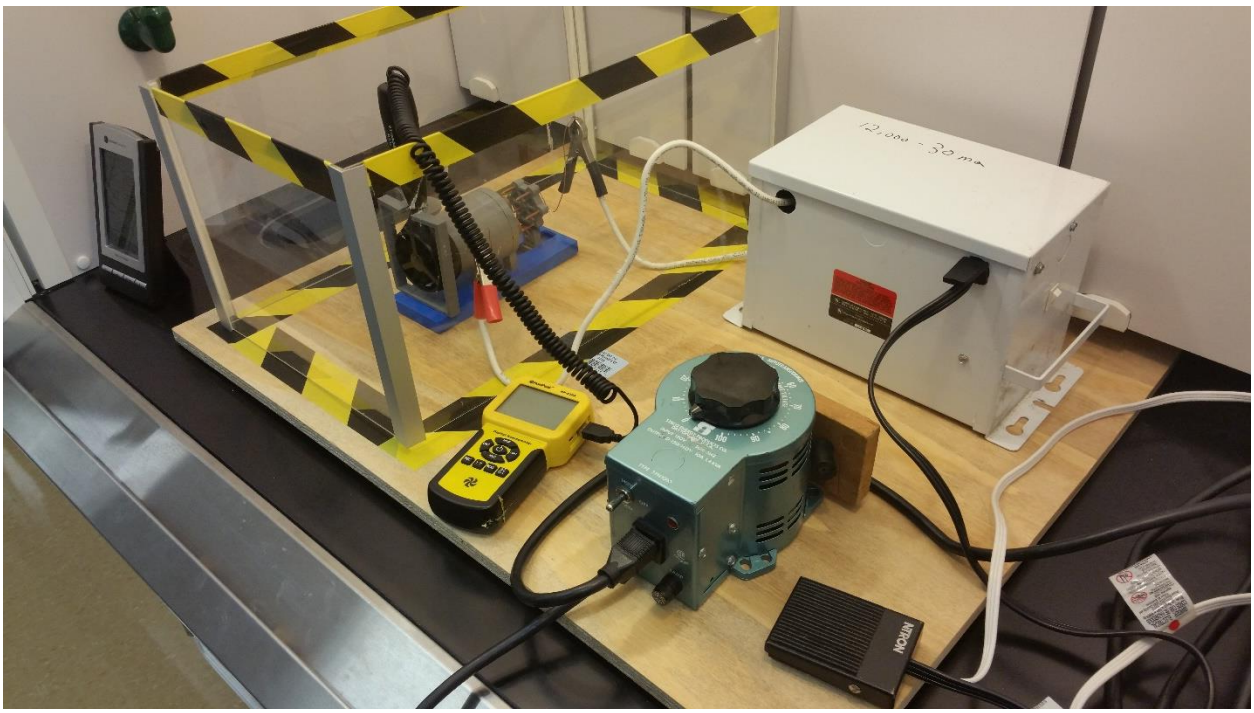

Figure 1: Final Prototype Ionic Propulsion Engine – Testing Assembly

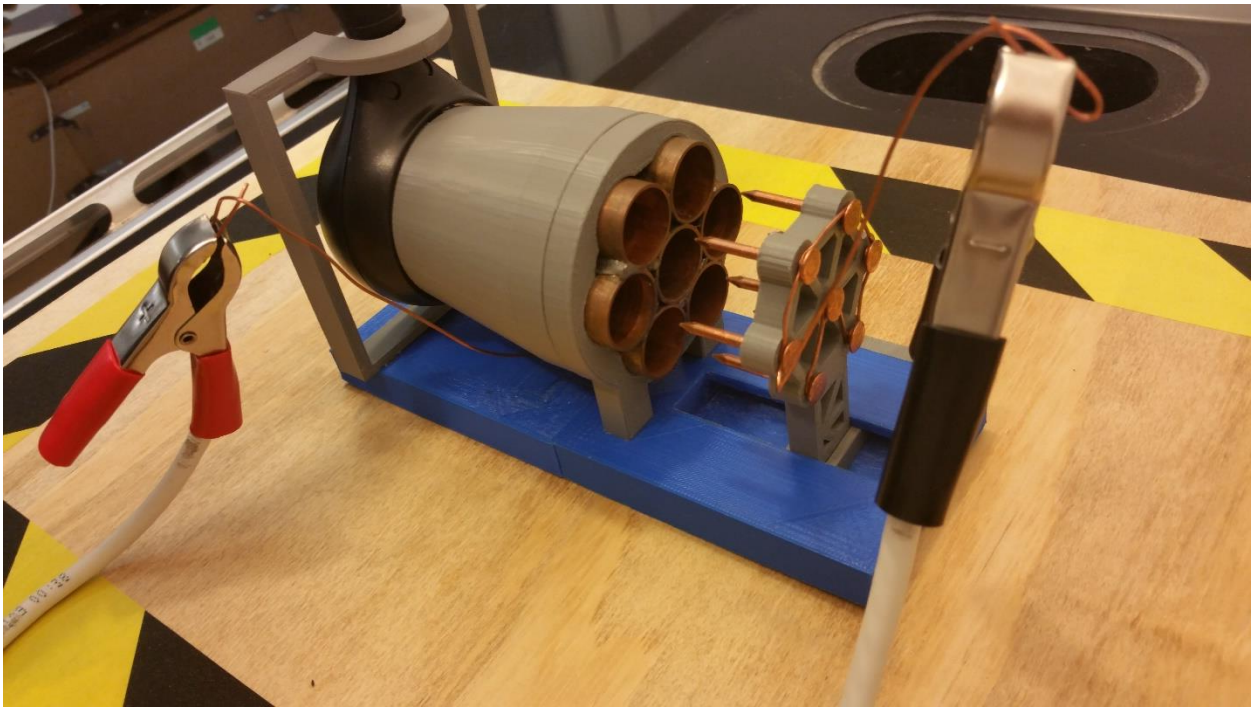

Figure 2: Final Prototype Ionic Propulsion Engine – Electrode Array

References

Cipolla, J. (2015). *Variable Specific Impulse Magnetoplasma Rocket (VASIMR) Propulsion*. Retrieved from http://www.aerorocket.com/PlasmaRocket.html

Duarte, J. (2015, September 18). *Ion Thruster*. Retrieved from http://www.elab-hackerspace.org/2015/09/18/ion-thruster/

Goebel, D. M., & Katz, I. (2008). *Fundamentals of Electric Propulsion: Ion and Hall thrusters* (Vol. 1). John Wiley & Sons.

Jackson, J. D. (1976). *Classical electrodynamics* (2nd ed.). New York: John Wiley & Sons.

NASA – Ion Propulsion. (2016, January 11). Retrieved from http://www.nasa.gov/centers/glenn/about/fs21grc.html

Reifsnyder, A. (2015, August 27). *Build an Ionic Thruster like NASA Uses for Space Propulsion*. Retrieved from http://makezine.com/projects/ionic-thruster/